THE JOURNAL OF BIOLOGICAL CHEMISTRY
Vol. 279, No. 45, Issue of November 5, pp. 47115–47124, 2004

Printed in U.S.A.

Mechanisms of Dense Core Vesicle Recapture following "Kiss and Run" ("Cavicapture") Exocytosis in Insulin-secreting Cells*[S]

Received for publication, July 20, 2004, and in revised form, August 24, 2004
Published, JBC Papers in Press, August 25, 2004, DOI 10.1074/jbc.M408179200

Takashi Tsuboi‡‖, Harvey T. McMahon§, and Guy A. Rutter‡¶

From the ‡Henry Wellcome Laboratories for Integrated Cell Signalling and the Department of Biochemistry, School of Medical Sciences, University Walk, University of Bristol, Bristol BS8 1TD, United Kingdom and the §Medical Research Council, Laboratory of Molecular Biology, Hills Road, Cambridge CB2 2QH, United Kingdom

The molecular mechanisms underlying "kiss and run" or "cavicapture" exocytosis of dense core secretory vesicles are presently unclear. Although dynamin-1 has previously been implicated in the recapture process in neurons, the recruitment of this fission protein to a single exocytosing vesicle has not been examined in real time during peptide release from pancreatic β-cells. Imaged simultaneously in clonal insulin-secreting cells by dual color total internal reflection fluorescence microscopy, monomeric red fluorescent protein (mRFP)-tagged neuropeptide Y and green fluorescent protein (GFP)-tagged synaptotagmin-1 or synaptobrevin-2 rapidly diffused from sites of exocytosis, whereas the vesicle membrane protein phogrin and tissue plasminogen activator (tPA) were retained, consistent with fusion pore closure. Vesicle recovery frequently involved the recruitment of enhanced GFP-tagged dynamin-1, and GTPase-defective dynamin-1(K44E) increased the dwell time of tPA-mRFP at the plasma membrane. By contrast, recruitment of GFP chimeras of clathrin, epsin, and amphiphysin was not observed. Expression of dynamin-1(K535A), mutated in the pleckstrin homology domain, caused the apparent full fusion of vesicles, as reported by the additional release of tPA-mRFP (15-nm diameter) and enhanced GFP-tagged phogrin. We conclude that re-uptake of vesicles after peptide release by cavicapture corresponds to a novel form of endocytosis in which dynamin-1 stabilizes and eventually closes the fusion pore, with no requirement for "classical" endocytosis for retreat from the plasma membrane.

The regulated release of peptide hormones has classically been thought to require the full fusion of the dense core vesicle membrane with the plasmalemma, *i.e.* the formation a "fusion pore" that eventually collapses via an "omega" structure to permit the passage of intravesicular protein cargoes (1, 2). Indeed, release of insulin has been proposed to involve the release of the crystalline dense core (100–200-nm diameter) essentially as an intact structure (3, 4), an event almost certainly requiring full fusion (5, 6). Other data (7) have, however, questioned these views and suggested instead that a process akin to "kiss and run" fusion of synaptic vesicles (8) and termed "cavity recapture" ("cavicapture") by Henkel and Almers (9) and Taraska and Almers (10) or "porocytosis" (11) is involved in the exocytosis of dense core vesicles in neuroendocrine cells. In contrast to classical kiss-and-run, cavicapture allows the release of selected protein cargoes from dense core vesicles during transient fusion with the cell membrane (12). In neither process, however, does the vesicle flatten fully into the plasmalemma.

We recently demonstrated (13) that the release of the vesicle cargo protein neuropeptide Y (NPY)[1]-Venus (where Venus is a pH-insensitive mutant of yellow fluorescent protein) (14) as well as lower molecular mass molecules (15) does not involve the transfer into the plasma membrane of the vesicle membrane protein phogrin (phosphatase on the granule of insulin-containing cells). Indeed, using a statistical approach and monitoring the release of different vesicle membrane proteins and cargoes, we defined three distinct forms of kiss and run exocytosis (transient, mixed, and full). Similarly, Taraska *et al.* (16) demonstrated the partial release of another cargo protein, tissue plasminogen activator (tPA), whereas enhanced green fluorescent protein (EGFP)-tagged phogrin was retained on the membrane of the same vesicle in pheochromocytoma (PC12) cells.

Using capacitance measurements in chromaffin cells, Palfrey and co-workers (17) proposed that two kinetically and mechanistically distinct forms of endocytosis occur following exocytosis: a rapid form of endocytosis, which requires the function of dynamin-1, a GTPase associated with the binding of endocytotic vesicles, but not the coat protein clathrin, and a second, slower phase. Whereas the rapid form is strictly Ca^{2+}-dependent, the second phase of endocytosis involves clathrin and dynamin-2, but does not require an increase in intracellular Ca^{2+} concentration. Correspondingly, using static imaging approaches in fixed PC12 cell plasma membrane lawns, Jahn and co-workers (3) demonstrated that dynamin becomes associated preferentially with vesicles that have undergone uptake of high molecular mass fluid-phase markers and thus, presumably, cavicapture events. At present, however, it is unclear (i) at what stage during a single exocytotic event dynamin-1 is recruited, *i.e.* during or after peptide release and closure of a

* This work was supported in part by Wellcome Trust Project 062321 (Programme 067081/Z/02/Z) and grants from the Biotechnology and Biological Sciences Research Council, the Human Frontiers Science Program, and Diabetes UK (to G. A. R.). The costs of publication of this article were defrayed in part by the payment of page charges. This article must therefore be hereby marked "*advertisement*" in accordance with 18 U.S.C. Section 1734 solely to indicate this fact.

[S] The on-line version of this article (available at http://www.jbc.org) contains supplemental Movies 1–5.

¶ Recipient of a Wellcome Trust research leave fellowship. To whom correspondence should be addressed. Tel.: 44-117-954-6401; Fax: 44-117-928-8274; E-mail: g.a.rutter@bristol.ac.uk.

‖ Recipient of a Juvenile Diabetes Research Foundation International postdoctoral fellowship.

[1] The abbreviations used are: NPY, neuropeptide Y; tPA, tissue plasminogen activator; GFP, green fluorescent protein; EGFP, enhanced green fluorescent protein; VAMP2, vesicle-associated membrane protein-2 (synaptobrevin-2); TIRF, total internal reflection fluorescence; SNARE, soluble *N*-ethylmaleimide-sensitive factor attachment protein receptor; mRFP, monomeric red fluorescent protein; Syt1, synaptotagmin-1; LC, light chain; PH, pleckstrin homology; IA-2, insulinoma-associated protein-2; GTPγS, guanosine 5′-*O*-(3-thiotriphosphate).

transient fusion; (ii) whether the association of dynamin with the exocytosing vesicle affects the ultimate outcome of the event, *i.e.* the decision between "full fusion" and cavicapture (13); or (iii) whether dynamin recruitment occurs in neuroendocrine cells, including pancreatic β-cells.

By monitoring exocytosis using a *Descosoma* coral red fluorescent protein-synaptobrevin-2 (DsRed-VAMP2) chimera and endocytosis with dynamin-1-EGFP, we have previously shown that only ~20% of apparent exocytotic events appear to involve rapid endocytosis in PC12 cells (18). However, these earlier studies did not explore the recruitment of clathrin or other proteins involved in endocytosis, including the adaptor molecule epsin (19). The latter molecule is involved in binding adaptor protein-2 and subsequently the formation of a clathrin cage. Binding of epsin to the plasma membrane involves an interaction between the epsin N-terminal homology domain and phosphatidylinositol 4,5-bisphosphate generated as a signal for endocytosis (20). Insertion of epsin into the membrane then appears to cause membrane curvature (21), facilitating vesicle formation and recapture. Whether epsin plays a similar role in the re-uptake of dense core vesicles post-fusion is unclear, however.

Here, we have determined, using simultaneous total internal reflection fluorescence (TIRF) imaging of a range of vesicle cargoes and membrane proteins along with fluorescently labeled wild-type and mutant dynamins, whether vesicle recapture following transient fusion events capable of releasing peptide cargoes involves a simple reversal of the fusion process and the retention of vesicle-associated SNARE proteins within the vesicle membrane or the deployment of the classical endocytosis machinery. Using dual color TIRF microscopy (15), we imaged the behavior of fluorescently labeled SNARE proteins and dynamin-1 before, during, and after single exocytotic events in insulin-secreting pancreatic β-cells (MIN6).

Using this approach, we show for the first time in β-cells that the recruitment of dynamin-1-EGFP occurs frequently to sites of either NPY-monomeric red fluorescent protein (mRFP) or tPA-mRFP release. By contrast, other mediators of "classical" endocytosis, including epsin-EGFP and clathrin-EGFP, rarely migrate to these sites. Instead, vesicles in pancreatic β-cells participate in a more complete form of fusion, allowing the selective release of small molecular mass vesicle membrane proteins (VAMP2 and synaptotagmin-1 (Syt1)), but not phogrin, into the plasma membrane. Stabilization and closure of the fusion pore appear to involve the recruitment of dynamin, without the creation of a clathrin cage, consistent with the preservation of a fully curved vesicle prior to re-uptake. Therefore, the present findings identify cavicapture as a novel form of endocytosis in pancreatic β-cells, with no apparent requirement for catalyzed membrane curvature.

EXPERIMENTAL PROCEDURES

Expression Vectors—Dynamin-1-EGFP, dynamin-1(K44E)-EGFP, dynamin-1(K535A)-EGFP, EGFP-VAMP2, NPY-mRFP, phogrin-EGFP, and epsin-1-EGFP were constructed as described previously (13, 15, 18, 22, 23). Clathrin light chain (LC)-EGFP was generated by excising the clathrin LC open reading frame from clathrin LC-DsRed (a gift from Dr. Wolfhard Almers) and subcloning it into the EcoRI/KpnI sites of the pEGFP-N1 vector (Clontech). To generate cDNA encoding rat tPA fused to mRFP, we removed the coding sequence of EGFP from tPA-EGFP (a gift from Dr. Beth Scalettar) by digestion with SacII/NotI and replaced it with the corresponding fragment from NPY-mRFP.

Rat cDNA encoding amphiphysin-1 was amplified by PCR with forward primer 5′-CTCGAGATGGCCGACATCAAGACGGG-3′ (with the XhoI site underlined) and reverse primer 5′-GAATTCTCTCCAGGCGCCGCGTGAA-3′ (with the EcoRI site underlined). The PCR product was digested with XhoI/EcoRI and inserted into the corresponding sites of the pEGFP-N1 expression vector. Rat cDNA encoding Syt1 was amplified by PCR with forward primer 5′-CTCGAGATGGTGAGTGCCAGTCATCCTGAG-3′ (with the XhoI site underlined) and reverse primer 5′-GAATTCTCTTCTTGACAGCCAGCATGGC-3′ (with the EcoRI site underlined). The PCR product was digested with XhoI/EcoRI and inserted into the corresponding sites of the pEGFP-N1 expression vector. To generate plasmids encoding dynamin-1 or dynamin-1(K535A), the open reading frame of dynamin-1 or dynamin-1(K535A) was amplified by PCR with forward primer 5′-GGATCCATGGGCAACCGCGGCATG-3′ (with the BamHI site underlined) and reverse primer 5′-AAGCTTTCAGGGGTCACTGATAGTGAT-3′ (with the HindIII site underlined). The PCR products were cleaved with BamHI/HindIII and subcloned into the pcDNA3.1(−) vector. The sequences of the inserts and the presence of the mutation were verified by automated DNA sequencing.

MIN6 Cell Culture—MIN6 β-cells (24) were used between passages 19 and 30 and grown in Dulbecco's modified Eagle's medium containing 15% (v/v) heat-inactivated fetal calf serum (Invitrogen, Paisley, United Kingdom), 25 mM glucose, 5.4 mM KCl, 2 mM glutamine, 50 μM β-mercaptoethanol, 100 IU/ml penicillin, and 100 mg/ml streptomycin. Cells were cultured in a humidified atmosphere at 37 °C with 5% CO_2. For dual color TIRF imaging (see below), MIN6 cells were plated on poly-L-lysine-coated high refractive index coverslips (n = 1.78; Olympus Optical Co., Tokyo, Japan). Cells were cotransfected with 2 μg (total) of plasmid DNA using LipofectAMINE 2000™ (Invitrogen) according to the manufacturer's instructions. Transfected cells were cultured in Dulbecco's modified Eagle's medium containing 25 mM glucose for 1 day and then in 3 mM glucose for an additional 16 h. Imaging was performed in modified Krebs-Ringer buffer (125 mM NaCl, 3.5 mM KCl, 1.5 mM $CaCl_2$, 0.5 mM NaH_2PO_4, 0.5 mM $MgSO_4$, 3 mM glucose, 10 mM HEPES, and 2 mM $NaHCO_3$ (pH 7.4) equilibrated with 19:1 O_2/CO_2). Stimulation with KCl was achieved by perfusion with Krebs-Ringer buffer containing 50 mM KCl and 75 mM NaCl.

Dual Color TIRF Microscopy—To selectively illuminate the plasma membrane and its associated vesicles, we used TIRF (also known as evanescent wave) microscopy (13, 25). An Olympus high numerical aperture objective lens (HR, Apochromatic, ×100, numerical aperture = 1.65, infinity-corrected) (26) was mounted on the nosepiece of a thermostatically controlled stage (37 °C; MC-60, Linkam, Surrey, United Kingdom) of an Olympus IX70 inverted microscope. A liquid (Cargille Laboratories, Cedar Grove, NJ) of high refractive index was used to couple the lens to the coverslip.

Fluorescent proteins of different colors were imaged simultaneously with an image splitter (Multispec MicroImager, Optical Insights, Santa Fe, NM) to separate the emission components of two fluorescent proteins into two channels, which were then projected as side-by-side images on a cooled charge-coupled device camera (640 × 480 pixels; IMAGO, Till Photonics) similar to that described previously (15). Images were acquired for 5 min at 2 Hz with a 150-ms exposure using TILLvisION software (Till Photonics) unless stated otherwise. EGFP and mRFP were both excited by a 488-nm laser line (argon ion laser, 30 milliwatts; Spectra-Physics) as described previously (15). A 565-nm dichroic mirror (Chroma 565DCXR) in the image splitter separated EGFP and mRFP fluorescence. EGFP passed through a 30-nm bandpass filter centered at 520 nm, and mRFP passed through a 630-nm long-pass filter.

Image Analysis—To analyze the data, single exocytotic events were manually selected. A 5 × 5-μm square region was centered on the brightest pixel of the first frame showing exocytosis. Onset of exocytosis was defined as the first frame showing a significant fluorescence increase of the vesicle. The same square was also placed on all other frames in the sequence. The same squares were used to select the corresponding point in the other color image using TILLvisION MicroImager macro software. The 5 × 5-μm squares thus defined were excised from the movies and stored as mini-stacks. A 1-μm diameter circle was centered on the fusing vesicles, and the average fluorescence intensity was measured. The circle was also transferred into the corresponding location in the other color image, and the average fluorescence intensity was measured. The local background was determined as the average fluorescence in a concentric annulus with a 4-μm outer diameter and subtracted. The colocalization (see Figs. 1 and 3) was calculated using MetaMorph colocalization software (Universal Imaging Corp., Media, PA).

Data Analysis—Data are given as means ± S.E. Comparisons between means were performed using one-tailed Student's t test for paired data with GraphPad Prism™ software. To calculate the time constant of decay and half-time, we normalized the NPY-mRFP and tPA-mRFP response to the same maximum amplitude. We then fitted a single exponential curve ($Y = y_0 + A_1\exp(-t/\tau_1)$, where y_0 is offset value of the amplitude, A_1 is the amplitude coefficient, t is time, and τ_1 is the

TABLE I
Molecular dimensions of vesicle proteins

Protein	Molecular mass	Residues	Volume	Dimensions[a]	-Fold[b]
	kDa		nm^3	*nm*	
EGFP	26.9	238	32.6	4.6 × 3.2 × 3.1	4.7
mRFP	25.9	225	31.3	4.6 × 3.1 × 3.0	4.5
Insulin	5.8	51	7.0	3.3 × 2.7 × 2.5	1
NPY	4.3	36	5.2	4.3 × 1.9 × 1.4	0.7
Human growth hormone	22.3	191	26.9	5.5 × 4.6 × 4.3	3.8
tPA	62.9	562	76.1	10–15 × 7 × 5[c]	10.9
VAMP2	12.6	115	15.2	10–15 × 1.3 × 1.1[c]	2.2
Vesicle side	0.2	2	0.2	1.3 × 1.1 × 0.2[d]	0.03
Syt1	47.4	421	57.3	9–11 × 2.9 × 2.8[c]	8.2
Vesicle side	5.6	53	6.8	2.9 × 2.8 × 1.1[d]	0.9
Phogrin	111.2	1003	134.7	ND[e]	19.2
Vesicle side	64.0	594	77.4	ND	11.1

[a] Protein dimensions were measured by Swiss-PdbViewer.
[b] These values reflect comparisons with insulin volume.
[c] These values are estimated dimensions. These crystal structures describe only 60–80% of the whole proteins.
[d] These values are estimated from the protein volume due to the lack of crystal structure determinations.
[e] ND, no determination of crystal structure.

decay constant) by nonlinear regression analysis, to give the decay time, using Origin 7™ (OriginLab, Northampton, MA).

RESULTS

Imaging Exocytotic Proteins in MIN6 Cells by Dual Color TIRF Microscopy—We labeled the insulin secretory vesicle membrane and cargo in clonal MIN6 β-cells by expressing phogrin-EGFP and NPY-mRFP, respectively (13, 22). The latter reporter is predicted to have molecular dimensions similar to those of monomeric insulin (~4-nm diameter) (Table I), but can be expressed in insulin-secreting cells without the complications of missorting and retention in the endoplasmic reticulum frequently observed with analogous insulin constructs (27).[2] Illuminated using the dual color TIRF microscope, most NPY-mRFP-positive vesicles (89.8 ± 4.6%, five cells) colocalized with phogrin-EGFP-positive vesicles (Fig. 1, *A–C*), confirming the efficient targeting of NPY-mRFP to phogrin/insulin-positive vesicles (22). Similarly, most Syt1-EGFP-labeled (78.4 ± 2.6%, five cells) and EGFP-VAMP2-labeled (92.3 ± 5.2%, five cells) structures colocalized with NPY-mRFP (Fig. 1, *D–F* and *G–I*). Finally, to verify whether another vesicle cargo protein, tPA-mRFP, was targeted to insulin-containing vesicles, we coexpressed this construct along with phogrin-EGFP. Most of the observed tPA-mRFP-positive vesicles (83.1 ± 4.3%, five cells) colocalized with phogrin-EGFP (Fig. 1, *J–L*). Therefore, at least beneath the plasma membrane, all of the green fluorescent protein (GFP)-tagged secretory vesicle membrane proteins and vesicle cargo proteins utilized were correctly targeted to insulin-containing dense core vesicles.

Dense Core Vesicles Release SNARE Proteins into the Plasma Membrane during and after Exocytosis—To observe the fate of secretory vesicle membrane proteins after peptide secretion, we overexpressed phogrin-EGFP and NPY-mRFP. Cell depolarization with 50 mM KCl caused the apparent release of NPY-mRFP, as monitored through a transient increase in fluorescence followed by diffusion away from the site of exocytosis, whereas the phogrin-EGFP signal from the same vesicle diminished only slightly, with a green fluorescent spot remaining throughout (Fig. 2*A* and Supplemental Movie 1). This result is consistent with previous data in INS-1 β-cells (15), and similar results have been obtained in PC12 cells (16). Fig. 2*B* shows the averaged fluorescence intensity measurement from several similar experiments. Whereas the majority of the NPY-mRFP fluorescence was lost rapidly from the vesicles (Fig. 2*B*, *closed circles*), phogrin-EGFP fluorescence remained nearly constant (*open circles*).

[2] T. Tsuboi and G. A. Rutter, manuscript in preparation.

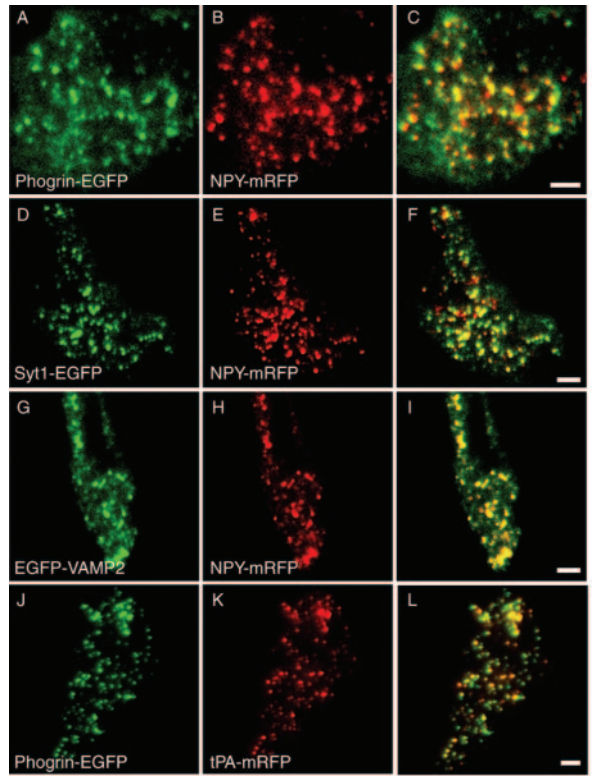

FIG. 1. **Colocalization of phogrin and SNARE proteins with secretory peptides in MIN6 cells.** *A*, dual color TIRF image of live MIN6 cells showing the distribution of phogrin-EGFP; *B*, image of NPY-mRFP fluorescence in the same cell; *C*, overlay of *A* and *B*; *D*, TIRF image of a live MIN6 cell showing Syt1-EGFP fluorescence; *E*, image of NPY-mRFP fluorescence in the same cell; *F*, overlay of *D* and *E*; *G*, TIRF image of EGFP-VAMP2 fluorescence in a live cell; *H*, image of NPY-mRFP fluorescence in the same cell; *I*, overlay of *G* and *H*; *J*, TIRF image of phogrin-EGFP fluorescence in a live cell; *K*, image of tPA-mRFP fluorescence in the same cell; *L*, overlay of *J* and *K*. *Scale bars* = 5 μm.

In all cases examined, the vesicular phogrin-EGFP remained associated with the vesicle and failed to spread into the plasma membrane for up to 4 min after exocytosis (data not shown). These data strongly suggest that, under these conditions, vesicles do not, or do not fully, collapse into the plasma membrane after exocytosis, a phenomenon that would be expected to lead to rapid diffusion away of phogrin-EGFP fluorescence.

tPA is a 63-kDa serine protease normally found in endothelial, PC12, and chromaffin cell granules (28, 29). We predicted

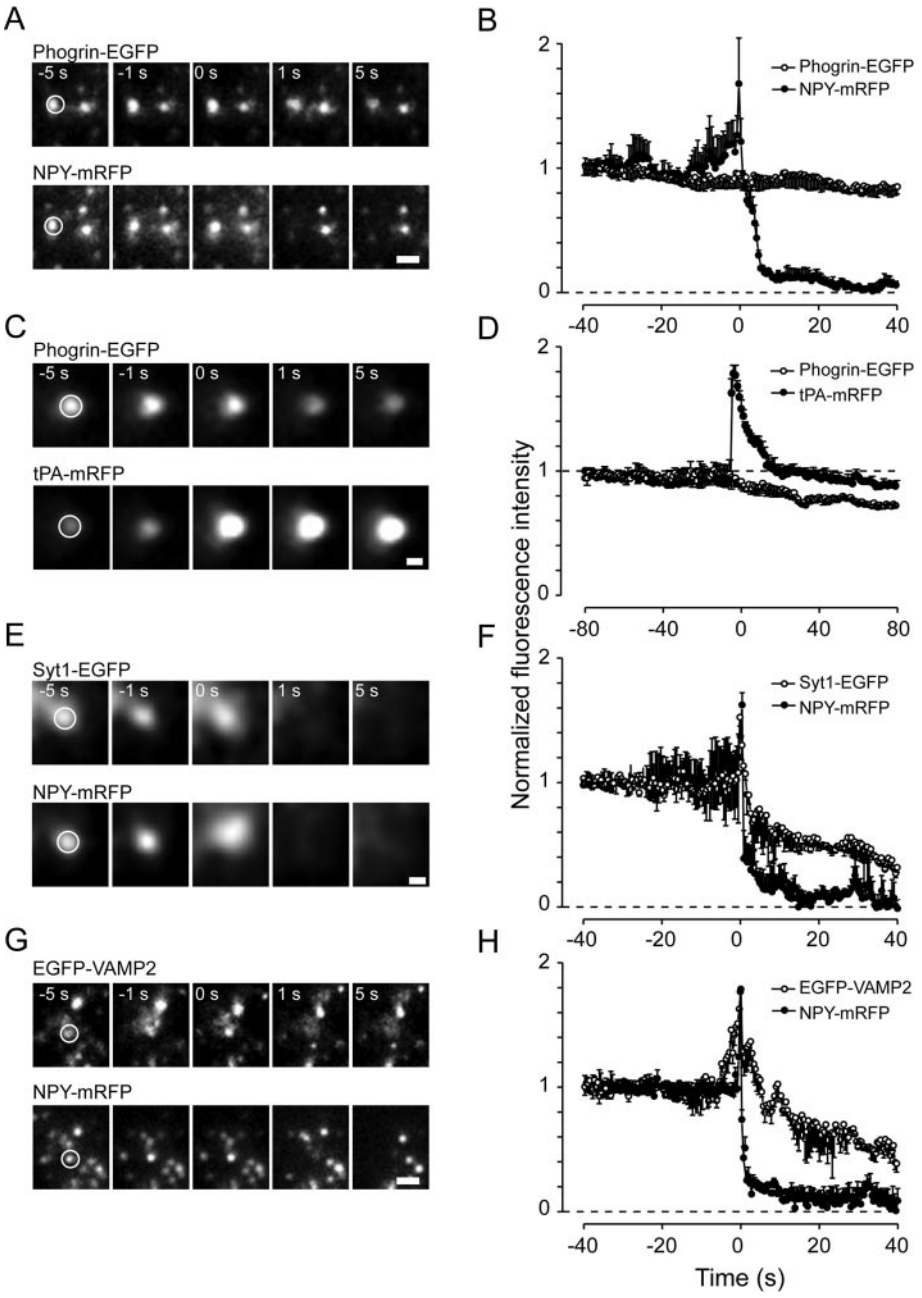

FIG. 2. **Phogrin and tPA remain on the secretory vesicles after exocytosis.** Five sequential dual color TIRF images show the behavior of single phogrin-EGFP and NPY-mRFP (*A*), phogrin-EGFP and tPA-mRFP (*C*), Syt1-EGFP and NPY-mRFP (*E*), and EGFP-VAMP2 and NPY-mRFP (*G*) vesicles after applying 50 mM KCl to the cell. The vesicle position before exocytosis is outlined by a *circle*. *Scale bars* = 1 μm. Averaged fluorescence intensity traces are shown of vesicles containing both phogrin-EGFP and NPY-mRFP (36 events, eight cells) (*B*), phogrin-EGFP and tPA-mRFP (24 events, six cells) (*D*), Syt1-EGFP and NPY-mRFP (38 events, seven cells) (*F*), and EGFP-VAMP2 and NPY-mRFP (35 events, eight cells) (*H*). Values are presented as the means ± S.E. of the normalized fluorescence intensity. Note that the *time scale* in *D* differs from those in *B*, *F*, and *H*. Supplemental Movie 1 includes QuickTime™ movies corresponding to *A*, *C*, *E*, and *G*.

that increases in the diameter of the fusion pore, up to and including complete collapse of the vesicle into the plasma membrane, should permit tPA-EGFP to be released completely from the secretory vesicle. However, previous experiments in PC12 cells showed that tPA-EGFP is usually retained in secretory vesicles (16) after exocytosis, arguing that full fusion events are rare.

To monitor the behavior of tPA and phogrin simultaneously in the same vesicle, we followed the dynamics of tPA-mRFP and phogrin-EGFP. As shown in Fig. 1 (*J–L*), nearly all tPA vesicles colocalized with the insulin vesicle marker phogrin in MIN6 cells. A representative tPA-mRFP and phogrin-EGFP fusion event is shown in Fig. 2*C* (see Supplemental Movie 1), and the corresponding time courses of fluorescence intensity change at the exocytosis site are shown in Fig. 2*D*. After an initial increase, tPA-mRFP fluorescence dimmed slowly, presumably reflecting either slow release of tPA or vesicle resealing and re-acidification (expected to quench mRFP fluorescence) (Fig. 2*D*, *closed circles*). Regardless of the mechanisms involved, it is evident that tPA-mRFP was retained in vesicles much longer than NPY-mRFP (Fig. 2*B*).

We next examined the fate of secretory vesicle-associated proteins during and after exocytosis. We expressed Syt1-EGFP with NPY-mRFP in MIN6 cells and observed the fluorescence intensity changes of these proteins during and after individual exocytotic events. Cell depolarization with 50 mM KCl caused Syt1-EGFP fluorescent spots to spread into the plasma membrane and then disappear, albeit more slowly than NPY-mRFP fluorescence (Fig. 2, *E* and *F*; and Supplemental Movie 1). Similarly, 50 mM KCl caused the spreading of the fluorescence of the SNARE protein, EGFP-VAMP2, from discrete vesicular structures into the plasma membrane, followed by a rapid disappearance of fluorescence (Fig. 2, *G* and *H*; and Supplemental Movie 1). This behavior is similar to that previously observed using VAMP2 fused to pH-sensitive GFP (synaptopHluorin) (13). These data indicate that a large proportion of the vesicle-associated protein complement is transferred into the plasma membrane after exocytosis.

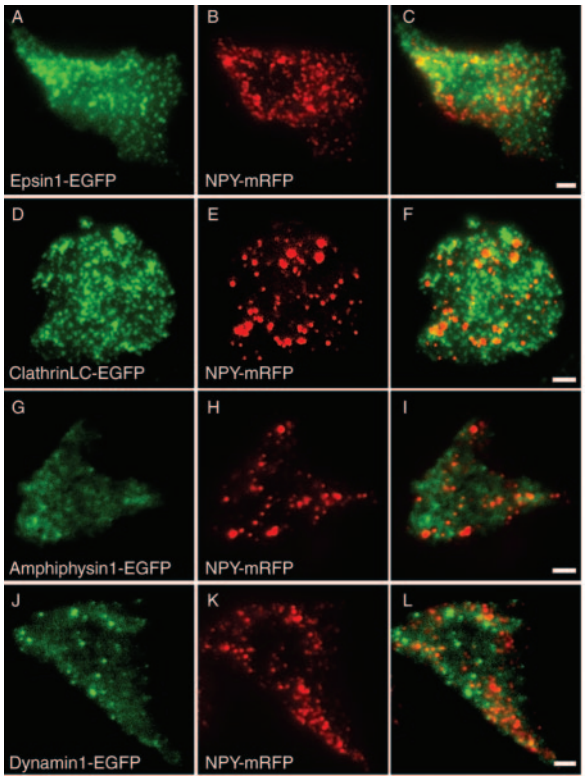

FIG. 3. **Colocalization of endocytotic proteins with NPY-mRFP in MIN6 beta cells.** *A*, TIRF image of epsin-1-EGFP fluorescence in a live cell; *B*, image of NPY-mRFP fluorescence in the same cell; *C*, overlay of *A* and *B*; *D*, TIRF image of clathrin LC-EGFP fluorescence in a live cell; *E*, image of NPY-mRFP fluorescence in the same cell; *F*, overlay of *D* and *E*; *G*, TIRF image of amphiphysin-1-EGFP fluorescence in a live cell; *H*, image of NPY-mRFP fluorescence in the same cell; *I*, overlay of *G* and *H*; *J*, TIRF image of dynamin-1-EGFP fluorescence in a live cell; *K*, image of NPY-mRFP fluorescence in the same cell; *L*, overlay of *J* and *K*. *Scale bars* = 5 μm.

Imaging of Endocytotic Proteins in MIN6 Cells by Dual Color TIRF Microscopy—Clathrin-mediated endocytosis is one of the primary mechanisms by which eukaryotic cells internalize nutrients, antigens, and growth factors and recycle receptors and vesicles (30). At the nerve terminal, clathrin-mediated endocytosis plays a crucial role in synaptic vesicle recycling (31–33). Many components of the clathrin-mediated endocytosis machinery have been identified, including epsin, amphiphysin, dynamin, and synaptojanin (34, 35).

To determine whether the recapture of dense core secretory vesicles following transient fusion events involves clathrin-dependent exocytosis, the dynamics of several endocytotic proteins during and after single exocytotic events were monitored by dual color TIRF microscopy. First, we determined the colocalization between endocytotic proteins and vesicle cargo proteins in resting MIN6 cells. Epsin-1-EGFP was apparent only in discrete puncta at the plasma membrane, which did not colocalize with NPY-mRFP (12.1 ± 2.4% colocalization, five cells) (Fig. 3, *A–C*). Similarly, punctate clathrin LC-EGFP structures failed to colocalize significantly with NPY-mRFP (11.3 ± 6.1%, five cells) (Fig. 3, *D–F*). In contrast, amphiphysin-1-EGFP displayed only cytosolic fluorescence (Fig. 3, *G–I*), whereas dynamin-1-EGFP puncta were less dense compared with clathrin LC-EGFP (Fig. 3, *J–L*) and likewise did not colocalize with NPY-mRFP (8.4 ± 2.5%, five cells). These data indicate that, at least beneath the plasma membrane, GFP-tagged endocytotic proteins are not localized to insulin-containing vesicles under resting conditions.

Several Cofactors in Clathrin-dependent Endocytosis Are Not Recruited to Sites of Exocytosis—Clathrin-dependent endocytosis is an ordered process involving the recruitment of adaptor complexes and accessory proteins onto the endocytosed membrane. This is rapidly followed by the assembly of clathrin coats, induction of membrane curvature, and fission of the mature bud (36). The phosphatidyl 4,5-bisphosphate-binding proteins epsin and amphiphysin are involved in the formation of clathrin coats and in synaptic vesicle endocytosis (37). To characterize the dynamics of endocytotic proteins during and after exocytosis, cells were cotransfected with epsin-1-EGFP and NPY-mRFP. Of those epsin-1-EGFP puncta present at the cell surface prior to stimulation, only a small proportion (<1%/min) disappeared into the cell after application of 50 mM KCl or moved laterally in linear trajectories parallel to the plane of the plasma membrane. Instead, the majority of the epsin-EGFP-labeled structures were unaffected by this treatment. Nevertheless, imaged simultaneously in the same cells, 50 mM KCl caused NPY-mRFP fluorescent spots to spread and then disappear, as expected, with no evident recruitment of epsin-1-EGFP to sites of apparent NPY-mRFP release (Fig. 4, *A* and *B*; and Supplemental Movie 2). In contrast to epsin-EGFP, amphiphysin-1-EGFP-labeled structures were rarely detected in the evanescent field beneath the plasma membrane, and no recruitment of amphiphysin-1-EGFP to NPY-mRFP release sites was evident for up to 4 min after the apparent release event (Fig. 4, *C* and *D*; and Supplemental Movie 2).

The above results suggested that vesicle recapture following transient fusion events is unlikely to be catalyzed by classical clathrin-dependent endocytosis in β-cells. However, to verify this directly, we observed the fate of clathrin LC-EGFP during and after individual exocytotic events. Whereas application of 50 mM KCl to the cells invoked the expected NPY-mRFP release events, neither the localization nor the movement of the clathrin LC-EGFP puncta was affected (Fig. 4, *E* and *F*; and Supplemental Movie 2). Taken together, the above findings indicate that the observed cavicapture NPY-mRFP release events do not involve clathrin-mediated endocytosis.

Dynamin-1 Translocates toward Exocytosing Vesicles—Dynamin is believed to oligomerize into rings around the neck of endocytotic vesicles, and this is thought to play a crucial function in the nanomechanics of membrane fission (38). Given the well established role of this GTPase in a variety of endocytotic processes (39–41), it was of interest to determine whether dynamin may play a role in the recapture of insulin-secreting vesicles after cavicapture exocytosis. We first determined whether dynamin may be present at sites where secretory vesicles are undergoing exocytosis and, if so, whether a correlation exists between the presence of dynamin and vesicle recapture. After stimulation with KCl to prompt NPY-mRFP release, the appearance in the evanescent field of dynamin-1-EGFP was clearly apparent (Fig. 5, *A* and *B*; and Supplemental Movie 3). After cell stimulation, the average appearance time at the plasma membrane of fluorescent spots containing dynamin-1-EGFP was ~16 s (16.4 ± 0.6 s, eight cells). Approximately 43% (43.4 ± 2.4%, six cells) of all exocytosed vesicles colocalized with dynamin after stimulation, with a significant change in the extent of colocalization from that observed prior to stimulation of the cells. This observation is similar to previous findings in PC12 cells (3, 18).

We next tested whether the dynamin GTPase domain mutant dynamin-1(K44E)-EGFP might change the recruitment kinetics of dynamin-1 to the exocytosis site. This mutant has previously been shown to be defective in vesicle scission such that the necks of budding vesicles continue to grow longer with time (38, 42, 43). Following cell stimulation, fluorescent spots containing dynamin-1(K44E)-EGFP appeared slowly at sites of NPY-mRFP release (Fig. 5*C* and Supplemental Movie 3). About

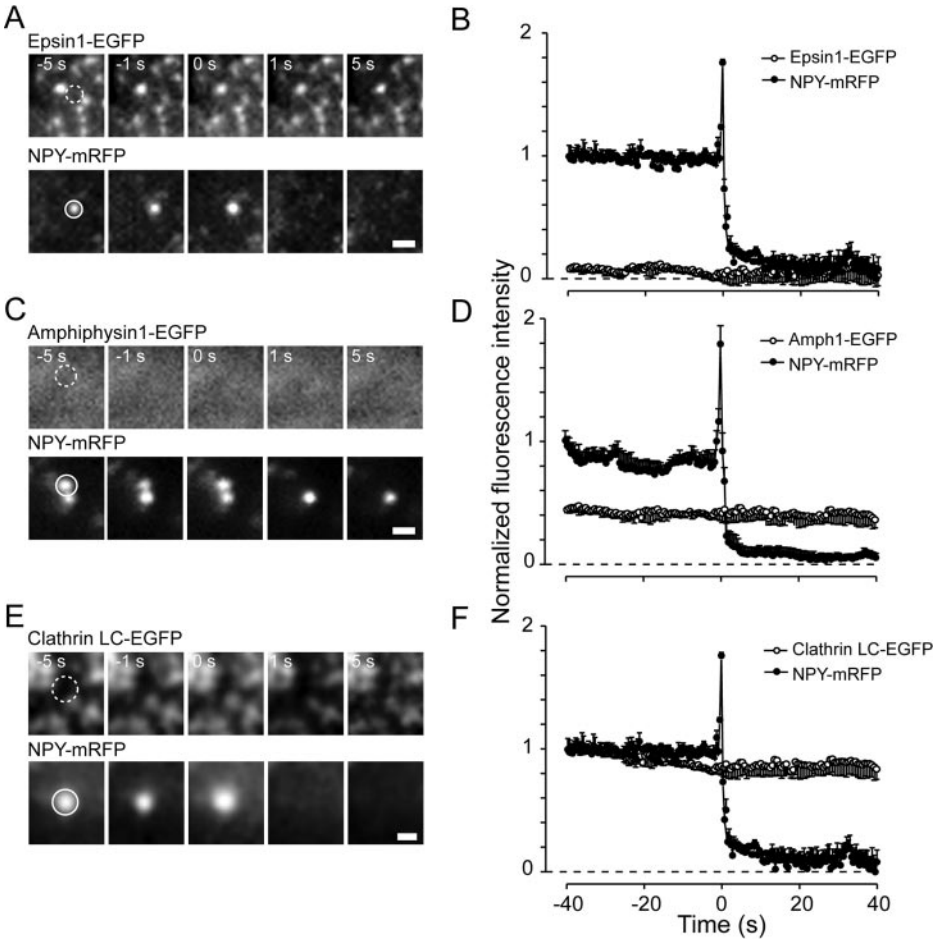

FIG. 4. **Absence of clathrin-dependent endocytotic proteins at sites of exocytosis.** Five sequential dual color TIRF images demonstrate the behavior of single epsin-1-EGFP and NPY-mRFP (*A*), amphiphysin-1-EGFP and NPY-mRFP (*C*), and clathrin LC-EGFP and NPY-mRFP (*E*) vesicles after applying 50 mM KCl to the cells. The vesicle position before exocytosis is outlined by a *circle*. *Scale bars* = 1 μm. Averaged fluorescence intensity traces are shown of vesicles containing both epsin-1-EGFP and NPY-mRFP (25 events, six cells) (*B*), amphiphysin-1 (*Amph1*)-EGFP and NPY-mRFP (21 events, six cells) (*D*), and clathrin LC-EGFP and NPY-mRFP (25 events, five cells) (*F*). Values are presented as the means ± S.E. of the normalized fluorescence intensity. Supplemental Movie 2 includes QuickTime™ movies corresponding to *A*, *C*, and *E*.

38% (38.3 ± 4.5%, six cells) of all exocytosed vesicles colocalized with dynamin-1(K44E)-EGFP spots after stimulation, a value identical to that obtained in cells expressing dynamin-1-EGFP (see above). The appearance of dynamin-1(K44E)-EGFP spots at sites of NPY-mRFP release was followed by a gradual decrease in fluorescence intensity (Fig. 5*D*), although detectable green fluorescence remained at the majority of the release sites for at least 4 min after exocytosis (data not shown).

Next, we determined whether the dynamin pleckstrin homology (PH) domain mutant dynamin-1(K535A)-EGFP might change the recruitment kinetics of dynamin-1 to the exocytosis site. Overexpression of a dynamin construct lacking its entire PH domain has been shown to block endocytosis completely, suggesting that dynamin interaction with phosphoinositides is essential for membrane capture (23, 39, 44). Correspondingly, dynamin-1(K535A)-EGFP was poorly recruited to NPY-mRFP release sites (Fig. 5*F* and Supplemental Movie 3).

Dynamin-1 Regulates the Apparent Diameter of the Fusion Pore—The results described so far suggest that cavicapture exocytosis may be regulated by dynamin-1. Given the expected behavior of dynamin-1 to accumulate around the neck of an endocytosing vesicle, we determined whether alteration of dynamin function, achieved by overexpression of dynamin-1(K44E), dynamin-1(K535A), or amphiphysin-1, all likely to bind to key interacting partners of endogenous dynamin, might change the diameter of the fusion pore and thus change the kinetics of tPA or NPY release. Although a high resolution structure for mRFP is not yet available, by analogy with that of GFP, the diameter of a single NPY-mRFP molecule can be predicted to be ~4 nm, a value close to that of an insulin monomer (45). By contrast, the diameter of tPA (~63 kDa) (Table I) (46) is expected to be approximately three times greater, *i.e.* 10–15 nm (note that the likely compact cylindrical structure of mRFP (<5-nm diameter) means that the presence of the latter fluorescent molecule has little effect on the above calculations). Overexpression of dynamin-1(K44E)-EGFP, dynamin-1(K535A)-EGFP, or amphiphysin-1-EGFP did not affect NPY-mRFP release kinetics (Fig. 6*A*), suggesting that either (i) the diameter of the fusion pore created in the absence of overexpressed dynamin-1 was at least 5 nm or (ii) the above mutants exerted no effect on fusion pore diameter.

By contrast, overexpression of either dynamin-1(K44E)-EGFP or amphiphysin-1-EGFP altered and prolonged the kinetics of tPA-mRFP release (Fig. 6*B*), although no release of tPA-mRFP from vesicles was apparent, as indicated by return to pre-exocytosis fluorescence levels after the upstroke of fluorescence increase. Under these conditions, it would therefore appear that fusion pore closure was slowed, but not completely inhibited, by interference with dynamin function. By contrast, in dynamin-1(K535A)-EGFP-overexpressing cells, tPA-mRFP fluorescence quickly dimmed after the onset of a tPA-mRFP release event and then decreased to below basal (pre-event) levels (Fig. 6*B*, *open diamonds*; and Supplemental Movie 4). Calculation of the time required to achieved 50% of the maximum amplitude (half-time) and the rate of spike fade taken from the adjusted exponential decay (decay time) from the traces of tPA-mRFP fluorescence intensity change revealed that dynamin-1(K44E)-EGFP and amphiphysin-1-EGFP significantly prolonged both parameters (Fig. 6, *C* and *D*). In contrast, dynamin-1(K535A)-EGFP significantly shortened both. The most straightforward interpretation of these data is that disruption of dynamin function changes the kinetics of fusion pore opening and/or closing and allows the formation of a fusion pore that is sufficiently wide to permit the release of

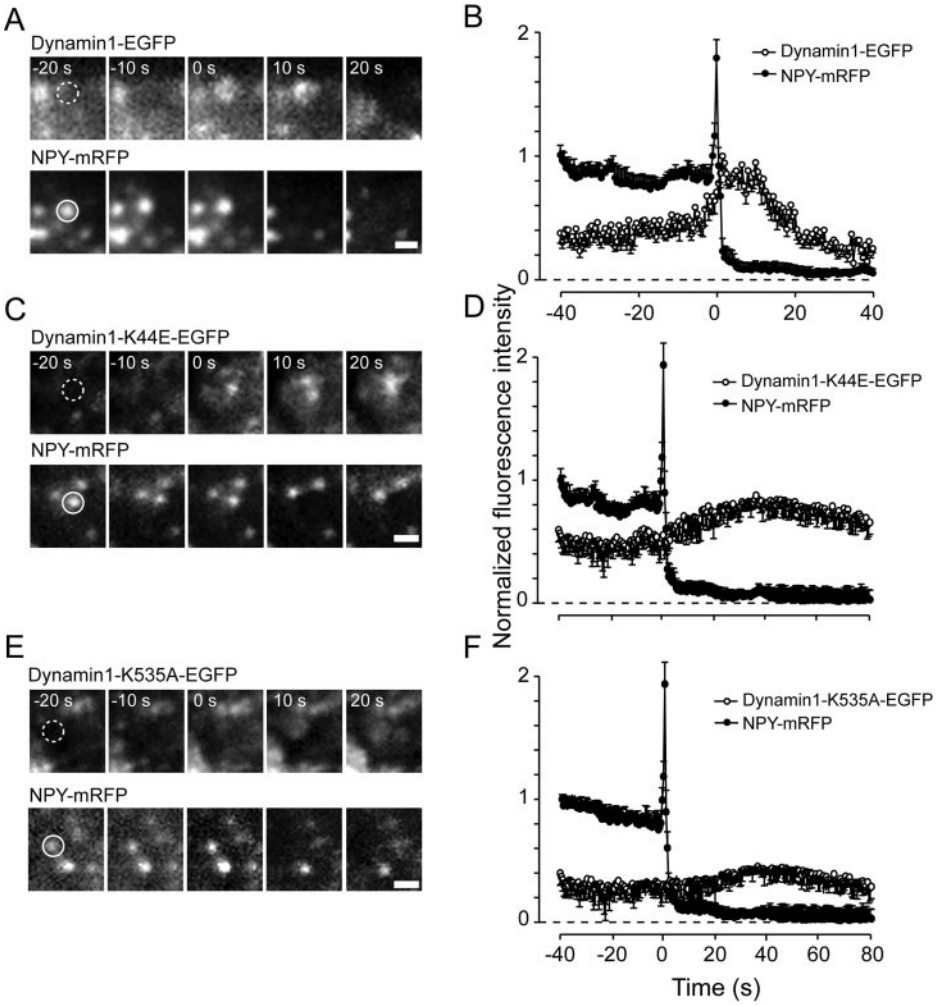

FIG. 5. **Dynamin-1 recruitment to NPY-mRFP release sites.** Five sequential dual color TIRF images demonstrate the behavior of single dynamin-1-EGFP and NPY-mRFP (*A*), dynamin-1(K44E)-EGFP and NPY-mRFP (*C*), and dynamin-1(K535A)-EGFP and NPY-mRFP (*E*) vesicles after applying 50 mM KCl to the cells. The vesicle position before exocytosis is outlined by a *circle*. *Scale bars* = 1 μm. Averaged fluorescence intensity traces are shown of vesicles containing both dynamin-1-EGFP and NPY-mRFP (34 events, eight cells) (*B*), dynamin-1(K44E)-EGFP and NPY-mRFP (37 events, eight cells) (*D*), and dynamin-1(K535A)-EGFP and NPY-mRFP (39 events, eight cells) (*F*). Values are presented as the means ± S.E. of the normalized fluorescence intensity. Supplemental Movie 3 contains QuickTime™ movies corresponding to *A*, *C*, and *E*.

tPA-mRFP, *i.e.* >10 nm, as well as the release of the membrane protein phogrin-EGFP.

The release of phogrin-EGFP from sites of exocytosis of other vesicle cargoes and vesicle membrane proteins was not detected in previous studies (13, 15, 16, 22), arguing against the full fusion of the vesicle and plasma membrane. On the other hand, it is formally possible that retention of phogrin at the site of exocytosis may occur despite full fusion as a result of the selective tethering of phogrin (note that these two possibilities cannot be resolved optically at the resolution of a light microscope). However, if this were the case, it would be predicted that prolongation of the fusion pore open state and/or diameter by dynamin-1(K535A) would not affect the release of phogrin-EGFP or lead to its diffusion into the plasma membrane. In line with previous findings (13, 15, 16, 22) and the results shown in Fig. 2*B*, 50 mM KCl stimulation of cells expressing only wild-type dynamin-1 caused a small diminution of phogrin-EGFP signals, and a fluorescent spot remained throughout the acquisition period (Fig. 7*B* and Supplemental Movie 5). In contrast, after overexpression of dynamin-1(K535A), events in which phogrin-EGFP-containing fluorescent spots spread completely into the plasma membrane and then disappeared were clearly evident (Fig. 7*D* and Supplemental Movie 5).

DISCUSSION

The principal aim of this study was to identify the mechanisms by which dense core secretory vesicles can fuse reversibly with the plasma membrane while still permitting the release of both soluble and membrane-bound protein cargoes. A key goal was therefore to define, by high speed imaging, the kinetics of the recruitment to the exocytosing vesicle of dynamin, previously implicated in cavicapture exocytosis in neuronal cells by both imaging (3) and electrophysiological measurements (17, 39, 47).

To achieve this, we used dual color TIRF microscopy to monitor simultaneously the behavior of multiple vesicle cargoes during individual secretory events. In a recent study (13), we demonstrated that VAMP2 diffuses rapidly from the site of exocytosis into the plasma membrane, whereas phogrin remains associated with the vesicle membrane (13, 15). We have shown here that the larger vesicle cargo protein tPA-mRFP remained within the intact vesicle during *bona fide* fusion events as reported by the transient increase in the fluorescence of the latter, likely to be caused by a cycle of vesicle alkalization and re-acidification. Furthermore, we have shown here for the first time that the recruitment of dynamin occurred very rapidly after exocytosis in endocrine cells, an observation not formerly possible in studies at fixed time points in PC12 cells (3). In our previous *in vivo* imaging studies using PC12 cells (18), we found that dynamin was recruited to sites of DsRed-VAMP2 release relatively rarely (~20% of events), in contrast to the recruitment of dynamin-1 to sites of NPY-Venus release in β-cells (43%). It also follows that, in β-cells, full vesicle fusion events (*i.e.* complete merger of vesicle and plasma membranes and the formation of an omega structure) are unlikely to occur. Moreover, given that the fusion pore apparently remains sufficiently small that tPA-mRFP (diameter likely to be between 10 and 15 nm as a monomer or between 20 and 30 nm as a dimer) (Table I) is retained, it would appear highly unlikely

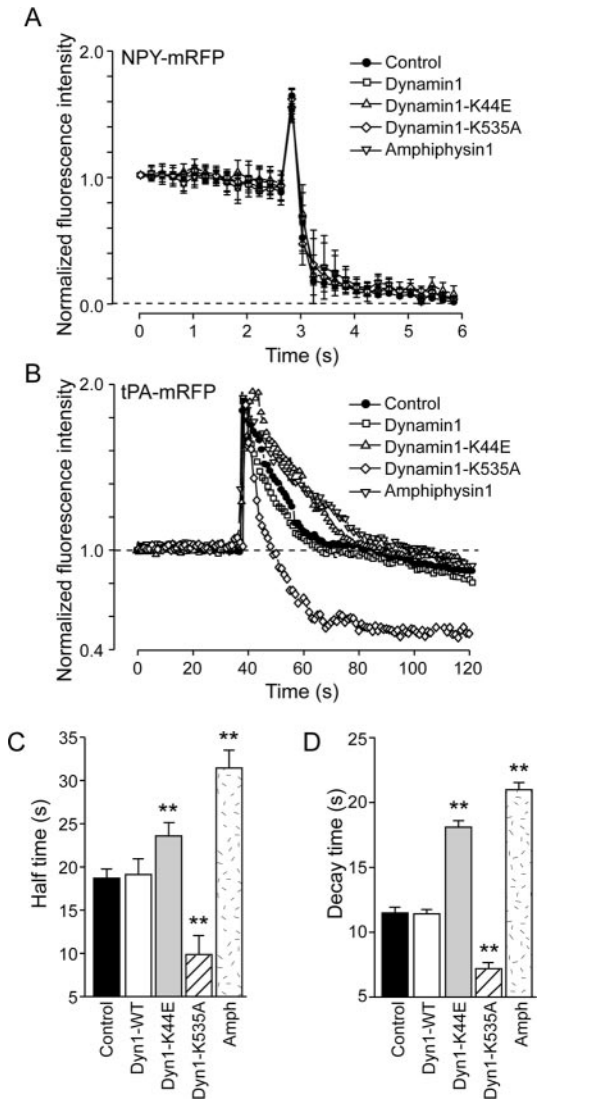

FIG. 6. **Disruption of dynamin function changes the kinetics of tPA-mRFP release.** Shown are the results from the analysis of fluorescence intensity changes in a single NPY-mRFP or tPA-mRFP vesicle coexpressed with dynamin-1-EGFP, dynamin-1(K44E)-EGFP, dynamin-1(K535A)-EGFP, or amphiphysin-1-EGFP. *A* and *B*, effect of high $[K^+]$ stimulation on the fluorescence intensity changes in NPY-mRFP and tPA-mRFP, respectively; *C*, half-time of fluorescence intensity in tPA-mRFP-expressing vesicles; *D*, decay time of fluorescence intensity in tPA-mRFP-expressing vesicles. **, $p < 0.01$ compared with the control. Supplemental Movie 4 includes a QuickTime™ movie corresponding to *B*. *Dyn1-WT*, wild-type dynamin-1; *Amph*, amphiphysin-1.

that the crystalline core of insulin secretory vesicles (100–200-nm diameter) is ever released "en masse."

Importantly, we have shown that the recruitment of dynamin was not associated with the recruitment to the exocytosing vesicle of other proteins usually involved in the execution of classical endocytosis in all cell types, including clathrin and epsin. The latter are essential to the formation of a "clathrin triskeleton," which is believed to aid membrane curvature and pinching off of an endocytotic vesicle. It seems likely that, in the case of cavicapture, it is unnecessary to impose further curvature to an already spherical vesicle. Instead, by ensuring fission of the transiently interacting vesicle and plasma membranes, dynamin action is presumably sufficient to ensure vesicle recapture and re-uptake by presently undefined mechanisms, which may include the recruitment of actin (48) and/or retrograde motor proteins such as dynein (49). Thus, we have defined here a novel form of (exocytosis-coupled) endocytosis, with both common and unique characteristics with respect to the classical endocytic pathway.

Takahashi *et al.* (6) employed a two-photon microscope to observe pancreatic islets and showed that stimulation in the presence of a fluorescent tracer results in the abrupt appearance of small omega shape fluorescent spots at the plasma membrane and then their rapid disappearance. Ma *et al.* (5) employed confocal and TIRF microscopy and extended the former observation. The latter authors simultaneously imaged the GFP-tagged secretory vesicle membrane protein syncollin and a fluorescent tracer during and after exocytosis and showed that the disappearance of omega shape fluorescent spots corresponds with the fusion of syncollin-GFP to the plasma membrane. Therefore, they concluded that the majority of insulin exocytosis occurs by full fusion (5). However, in neither of the above studies was the fate of other secretory vesicle membrane proteins (*e.g.* phogrin) monitored after the disappearance of omega shape fluorescent spots. In our view, in the absence of such recordings of the fate of the vesicle membrane itself, it is very difficult to conclude that the vesicle membrane actually collapses into the plasmalemma. Indeed, monitoring of the lipophilic dye FM4-64 simultaneously with NPY-EGFP in PC12 cells revealed that, even though membrane lipids rapidly equilibrate between the vesicle and plasma membrane, the observed secretory events (involving NPY-EGFP release) are usually transient and result in closure of the fusion pore, as assessed separately using a combination of GFP-phogrin and FM4-64 (10). We would emphasize that several other factors could affect the behavior of soluble vesicle markers such as sulforhodamine B and rhodamine-dextran, as used in the studies of Takahashi *et al.* (6) and Ma *et al.* (5), respectively. In particular, recent studies suggest that insulin and chromaffin vesicles possess ClC3 Cl^- channels, which regulate vesicular Cl^- fluxes and peptide dissolution during exocytosis (45, 50). These Cl^- fluxes could conceivably flush out the fluorescent dye during exocytosis, giving the appearance of a flattening vesicle.

An additional conclusion that flows from our own work is that it is likely that the insulin core must dissociate into smaller units (monomers or dimers) prior to passage through the fusion pore. However, it should be stressed that, although high resolution electron microscopy indicates that native GFP, expressed after fusion with a secretory pathway signal peptide, becomes incorporated into the crystalline dense core of the vesicle (51), it has yet to be established definitively whether either NPY-mRFP or tPA-mRFP exists within the dense core or vesicle "halo" in MIN6 cells.

We have also extended earlier observations on the release of VAMP2 (13, 18) by showing that another vesicle-associated protein, Syt1, moved rapidly from the site of exocytosis during NPY-mRFP release (Fig. 2). How is this discrimination between membrane proteins achieved? Although we cannot eliminate the possibility that the behavior of the overexpressed proteins may not reflect with absolute fidelity that of the endogenous proteins, we suspect that VAMP2 and Syt1, but not phogrin, are free to diffuse since they lack any tethering molecule(s) on the vesicle membrane. Indeed, several proteins that bind to both phogrin (IA-2β) and the closely related insulinoma-associated protein IA-2 have been identified by the use of yeast two-hybrid analysis and co-immunoprecipitation. These include β_{IV} spectrin and the PDZ domains of β_2-syntrophin. Moreover, Solimena and co-workers (52, 53) have postulated that IA-2 may link the secretory vesicles with the actin cytoskeleton through its association with β_{IV} spectrin or β_2-syntrophin, and this may also be involved in the retention of phogrin on dense core vesicles. For instance, in IA-2-deficient mice, only 50–60% of the normal amount of insulin is secreted from isolated pancreatic islets upon glucose stimulation *in*

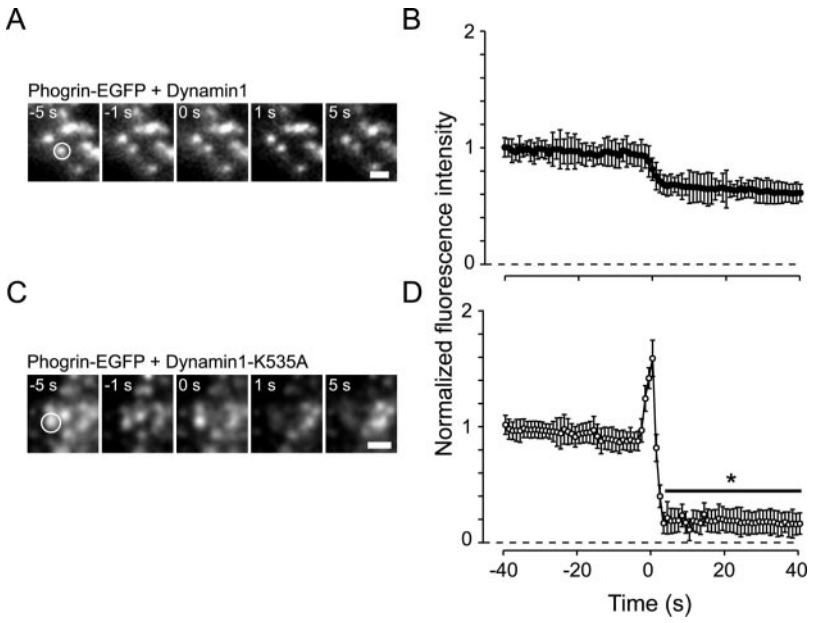

FIG. 7. **Dynamin-1(K535A) leads to release of tPA-EGFP and phogrin-EGFP.** Five sequential TIRF images demonstrate the behavior of a single phogrin-EGFP vesicle coexpressed with wild-type dynamin-1 (*A*) and dynamin-1(K535A) (*C*) after applying 50 mM KCl to the cells. The vesicle position before exocytosis is outlined by *circle*. *Scale bars* = 1 μm. Averaged fluorescence intensity traces are shown of vesicles containing both dynamin-1 and phogrin-EGFP (24 events, six cells) (*B*) and dynamin-1(K535A) and phogrin-EGFP (32 events, seven cells) (*D*). Values are presented as the means ± S.E. of the normalized fluorescence intensity. *, $p < 0.05$ compared with pre-stimulatory fluorescence. Supplemental Movie 5 includes QuickTime™ movies corresponding to *A* and *C*.

vitro. Moreover, IA-2-deficient mice display abnormal glucose tolerance (54). These findings suggest that IA-2 family members may play an important role in the regulated release of insulin, consistent with their enrichment in the secretory vesicles of neurons (55, 56).

We noted here that, after expression of dynamin-1 mutated in the PH domain, both tPA and phogrin were able to leave the site of vesicle fusion, in contrast to the situation in control cells. Whether such events correspond to complete merger of the vesicle and plasma membranes is uncertain, however, given that, after the purging of fluorescently labeled vesicle membrane proteins, the fate of the "ghost" membrane was not monitored in this study. However, the principal binding partners of phogrin (see above) are likely to be localized to the cytosolic surface of the vesicle and thus insensitive to relatively small changes in fusion pore diameter. We therefore suspect that the observed release of phogrin is most compatible with complete vesicle collapse after expression of mutant dynamin.

An important feature of cavicapture exocytosis is that SNARE complexes that form during the initial vesicle fusion do not need to be immediately unpaired, an energetically highly unfavorable process and therefore one likely to occur very slowly (Fig. 8*A*) (57). Instead, dynamin recruitment appears to stabilize the pore, allowing the diffusion of paired SNARE complexes into the plasmalemma. Pore closure can then occur without any apparent requirement for the recruitment of epsin or other catalysts of membrane curvature or the formation of a clathrin cytoskeleton to force the curvature of an already spherical (*i.e.* essentially unchanged) vesicle (Fig. 4). Consistent with the above, overexpression of amphiphysin Src homology-3 domain or GTPγS to adrenal chromaffin cells inhibits quantal size measured by carbon fiber amperometry, whereas anti-dynamin-1 antibodies prevent "rapid endocytosis" (17). Likewise, GTPγS inhibits sulforhodamine uptake into PC12 cell granules (3), suggesting that dynamin regulates kiss and run or cavicapture exocytosis in each of these systems (47).

What are the likely advantages of cavicapture exocytosis for insulin release? Since the mixing of all membrane components with the cell surface is avoided, a vesicle may potentially revisit the membrane for a second round of exocytosis. For example, subsequent to a "transient" kiss and run event, which may lead to the release of only small vesicle cargoes (*e.g.* neurotransmitters including ATP, divalent metal ions, etc.) (13), a second event could conceivably follow in which the vesicle undergoes fuller fusion, culminating in peptide release. On the other hand, it would seem likely that vesicles whose peptide cargo content, including insulin, has been largely or completely depleted by cavicapture are then destined for lysosomal destruction, given that vesicle biosynthesis at the *trans*-Golgi network is likely to be the sole mechanism for the filling of vesicles with peptide cargo.

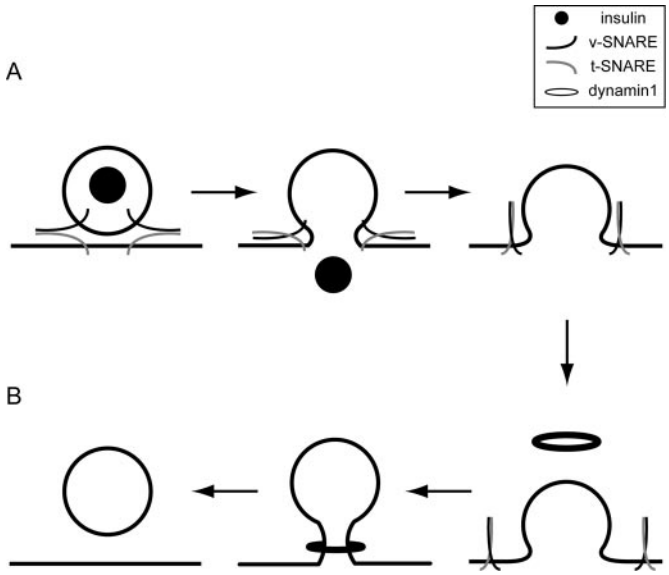

FIG. 8. **Fate of SNARE proteins during transient vesicle fusion (*A*) and role of dynamin-1 in vesicle recapture (*B*).** A new mechanism is shown whereby dynamin causes fission of the intact fused vesicle before collapse and intermixing with the plasma membrane. *v-SNARE*, vesicle SNARE; *t-SNARE*, target SNARE.

In conclusion, our findings provide direct evidence that dynamin-1 is a key element of cavicapture exocytosis. Elucidating the precise molecular mechanism of dynamin-1 recruitment to the fusing vesicle may provide further valuable insights into this form of exocytosis-coupled endocytosis.

Acknowledgments—We thank Katsuyuki Abe (Olympus Optical Co.) and Hitoshi Hatano (Olympus Optical Europe GmbH) for generous technical support; Drs. Wolfhard Almers, Andreas Jeromin, and Beth Scalettar for plasmids; and Philip D. Mountjoy for proofreading the manuscript.

REFERENCES

1. Lindau, M., and Almers, W. (1995) *Curr. Opin. Cell Biol.* **7,** 509–517
2. Zenisek, D., Steyer, J. A., Feldman, M. E., and Almers, W. (2002) *Neuron* **35,** 1085–1097
3. Holroyd, P., Lang, T., Wenzel, D., De Camilli, P., and Jahn, R. (2002) *Proc. Natl. Acad. Sci. U. S. A.* **99,** 16806–16811
4. Orci, L., Amherdt, M., Malaisse-Lagae, F., Rouiller, C., and Renold, A. E. (1973) *Science* **179,** 82–84
5. Ma, L., Bindokas, V. P., Kuznetsov, A., Rhodes, C., Hays, L., Edwardson, J. M., Ueda, K., Steiner, D. F., and Philipson, L. H. (2004) *Proc. Natl. Acad. Sci. U. S. A.* **101,** 9266–9271
6. Takahashi, N., Kishimoto, T., Nemoto, T., Kadowaki, T., and Kasai, H. (2002) *Science* **297,** 1349–1352
7. Valtorta, F., Meldolesi, J., and Fesce, R. (2001) *Trends Cell Biol.* **11,** 324–328
8. Ceccarelli, B., and Hurlbut, W. P. (1980) *J. Cell Biol.* **87,** 297–303
9. Henkel, A. W., and Almers, W. (1996) *Curr. Opin. Neurobiol.* **6,** 350–357
10. Taraska, J. W., and Almers, W. (2004) *Proc. Natl. Acad. Sci. U. S. A.* **101,** 8780–8785
11. Silver, R. B., Kriebel, M. E., Keller, B., and Pappas, G. D. (2001) *Biol. Bull.* (*Woods Hole*) **201,** 263–264
12. Rutter, G. A., and Tsuboi, T. (2004) *Neuroreport* **15,** 79–81
13. Tsuboi, T., and Rutter, G. A. (2003) *Curr. Biol.* **13,** 563–567
14. Nagai, T., Ibata, K., Park, E. S., Kubota, M., Mikoshiba, K., and Miyawaki, A. (2002) *Nat. Biotechnol.* **20,** 87–90
15. Tsuboi, T., Zhao, C., Terakawa, S., and Rutter, G. A. (2000) *Curr. Biol.* **10,** 1307–1310
16. Taraska, J. W., Perrais, D., Ohara-Imaizumi, M., Nagamatsu, S., and Almers, W. (2003) *Proc. Natl. Acad. Sci. U. S. A.* **100,** 2070–2075
17. Artalejo, C. R., Elhamdani, A., and Palfrey, H. C. (2002) *Proc. Natl. Acad. Sci. U. S. A.* **99,** 6358–6363
18. Tsuboi, T., Terakawa, S., Scalettar, B. A., Fantus, C., Roder, J., and Jeromin, A. (2002) *J. Biol. Chem.* **277,** 15957–15961
19. Chen, H., Fre, S., Slepnev, V. I., Capua, M. R., Takei, K., Butler, M. H., Di Fiore, P. P., and De Camilli, P. (1998) *Nature* **394,** 793–797
20. Lemmon, M. A. (2003) *Traffic* **4,** 201–213
21. Ford, M. G., Mills, I. G., Peter, B. J., Vallis, Y., Praefcke, G. J., Evans, P. R., and McMahon, H. T. (2002) *Nature* **419,** 361–366
22. Pouli, A. E., Emmanouilidou, E., Zhao, C., Wasmeier, C., Hutton, J. C., and Rutter, G. A. (1998) *Biochem. J.* **333,** 193–199
23. Vallis, Y., Wigge, P., Marks, B., Evans, P. R., and McMahon, H. T. (1999) *Curr. Biol.* **9,** 257–260
24. Miyazaki, J., Araki, K., Yamato, E., Ikegami, H., Asano, T., Shibasaki, Y., Oka, Y., and Yamamura, K. (1990) *Endocrinology* **127,** 126–132
25. Axelrod, D. (1981) *J. Cell Biol.* **89,** 141–145
26. Terakawa, S., Sakurai, T., and Abe, K. (1997) *Bioimages* **5,** 24
27. Pouli, A. E., Kennedy, H. J., Schofield, J. G., and Rutter, G. A. (1998) *Biochem. J.* **331,** 669–675
28. Lochner, J. E., Kingma, M., Kuhn, S., Meliza, C. D., Cutler, B., and Scalettar, B. A. (1998) *Mol. Biol. Cell* **9,** 2463–2476
29. Parmer, R. J., Mahata, M., Mahata, S., Sebald, M. T., O'Connor, D. T., and Miles, L. A. (1997) *J. Biol. Chem.* **272,** 1976–1982
30. Di Fiore, P. P., and De Camilli, P. (2001) *Cell* **106,** 1–4
31. Brodin, L., Low, P., and Shupliakov, O. (2000) *Curr. Opin. Neurobiol.* **10,** 312–320
32. Higgins, M. K., and McMahon, H. T. (2002) *Trends Biochem. Sci.* **27,** 257–263
33. Murthy, V. N., and De Camilli, P. (2003) *Annu. Rev. Neurosci.* **26,** 701–728
34. Huttner, W. B., and Schmidt, A. A. (2002) *Trends Cell Biol.* **12,** 155–158
35. Slepnev, V. I., and De Camilli, P. (2000) *Nat. Rev. Neurosci.* **1,** 161–172
36. Conner, S. D., and Schmid, S. L. (2003) *Nature* **422,** 37–44
37. Di Paolo, G., Sankaranarayanan, S., Wenk, M. R., Daniell, L., Perucco, E., Caldarone, B. J., Flavell, R., Picciotto, M. R., Ryan, T. A., Cremona, O., and De Camilli, P. (2002) *Neuron* **33,** 789–804
38. Marks, B., Stowell, M. H., Vallis, Y., Mills, I. G., Gibson, A., Hopkins, C. R., and McMahon, H. T. (2001) *Nature* **410,** 231–235
39. Artalejo, C. R., Lemmon, M. A., Schlessinger, J., and Palfrey, H. C. (1997) *EMBO J.* **16,** 1565–1574
40. Lee, E., and De Camilli, P. (2002) *Proc. Natl. Acad. Sci. U. S. A.* **99,** 161–166
41. Orth, J. D., Krueger, E. W., Cao, H., and McNiven, M. A. (2002) *Proc. Natl. Acad. Sci. U. S. A.* **99,** 167–172
42. Herskovits, J. S., Shpetner, H. S., Burgess, C. C., and Vallee, R. B. (1993) *Proc. Natl. Acad. Sci. U. S. A.* **90,** 11468–11472
43. Koenig, J. H., and Ikeda, K. (1989) *J. Neurosci.* **9,** 3844–3860
44. Klein, D. E., Lee, A., Frank, D. W., Marks, M. S., and Lemmon, M. A. (1998) *J. Biol. Chem.* **273,** 27725–27733
45. Barg, S., Olofsson, C. S., Schriever-Abeln, J., Wendt, A., Gebre-Medhin, S., Renstrom, E., and Rorsman, P. (2002) *Neuron* **33,** 287–299
46. Lamba, D., Bauer, M., Huber, R., Fischer, S., Rudolph, R., Kohnert, U., and Bode, W. (1996) *J. Mol. Biol.* **258,** 117–135
47. Graham, M. E., O'Callaghan, D. W., McMahon, H. T., and Burgoyne, R. D. (2002) *Proc. Natl. Acad. Sci. U. S. A.* **99,** 7124–7129
48. Merrifield, C. J., Feldman, M. E., Wan, L., and Almers, W. (2002) *Nat. Cell Biol.* **4,** 691–698
49. Varadi, A., Tsuboi, T., Johnson-Cadwell, L. I., Allan, V. J., and Rutter, G. A. (2003) *Biochem. Biophys. Res. Commun.* **311,** 272–282
50. Tsuboi, T., Kikuta, T., Sakurai, T., and Terakawa, S. (2002) *Biophys. J.* **83,** 172–183
51. Molinete, M., Lilla, V., Jain, R., Joyce, P. B., Gorr, S. U., Ravazzola, M., and Halban, P. A. (2000) *Diabetologia* **43,** 1157–1164
52. Berghs, S., Aggujaro, D., Dirkx, R., Jr., Maksimova, E., Stabach, P., Hermel, J. M., Zhang, J. P., Philbrick, W., Slepnev, V., Ort, T., and Solimena, M. (2000) *J. Cell Biol.* **151,** 985–1002
53. Ort, T., Maksimova, E., Dirkx, R., Kachinsky, A. M., Berghs, S., Froehner, S. C., and Solimena, M. (2000) *Eur. J. Cell Biol.* **79,** 621–630
54. Saeki, K., Zhu, M., Kubosaki, A., Xie, J., Lan, M. S., and Notkins, A. L. (2002) *Diabetes* **51,** 1842–1850
55. Cui, L., Yu, W. P., De Aizpurua, H. J., Schmidli, R. S., and Pallen, C. J. (1996) *J. Biol. Chem.* **271,** 24817–24823
56. Wasmeier, C., and Hutton, J. C. (1996) *J. Biol. Chem.* **271,** 18161–18170
57. Jahn, R., Lang, T., and Sudhof, T. C. (2003) *Cell* **112,** 519–533